



## Weak signal detection method based on novel composite multistable stochastic resonance

Shangbin Jiao(焦尚彬), Rui Gao(高蕊), Qiongjie Xue(薛琼婕), and Jiaqiang Shi(史佳强)

**Citation:** Chin. Phys. B, 2023, 32 (5): 050202. DOI: 10.1088/1674-1056/aca4bd

Journal homepage: <http://cpb.iphy.ac.cn>; <http://iopscience.iop.org/cpb>

**What follows is a list of articles you may be interested in**

---

### Meshfree-based physics-informed neural networks for the unsteady Oseen equations

Keyi Peng(彭珂依), Jing Yue(岳靖), Wen Zhang(张文), and Jian Li(李剑)

Chin. Phys. B, 2023, 32 (4): 040207. DOI: 10.1088/1674-1056/ac9cb9

### Local density of optical states calculated by the mode spectrum in stratified media

Ting Fu(傅廷), Jingxuan Chen(陈静瑄), Xueyou Wang(王学友), Yingqiu Dai(戴迎秋), Xuyan Zhou(周旭彦), Yufei Wang(王宇飞), Mingjin Wang(王明金), and Wanhua Zheng(郑婉华)

Chin. Phys. B, 2023, 32 (4): 040204. DOI: 10.1088/1674-1056/acaf2c

### Inverse stochastic resonance in modular neural network with synaptic plasticity

Yong-Tao Yu(于永涛) and Xiao-Li Yang(杨晓丽)

Chin. Phys. B, 2023, 32 (3): 030201. DOI: 10.1088/1674-1056/aca602

### Inhibitory effect induced by fractional Gaussian noise in neuronal system

Zhi-Kun Li(李智坤) and Dong-Xi Li(李东喜)

Chin. Phys. B, 2023, 32 (1): 010203. DOI: 10.1088/1674-1056/ac6332

### A self-adaptive stochastic resonance system design and study in chaotic interference

Lu Kang (鲁康), Wang Fu-Zhong (王辅忠), Zhang Guang-Lu (张光璐), Fu Wei-Hong (付卫红)

Chin. Phys. B, 2013, 22 (12): 120202. DOI: 10.1088/1674-1056/22/12/120202

---

# Weak signal detection method based on novel composite multistable stochastic resonance

Shangbin Jiao(焦尚彬)<sup>1</sup>, Rui Gao(高蕊)<sup>1,2,†</sup>, Qiongjie Xue(薛琼婕)<sup>1</sup>, and Jiaqiang Shi(史佳强)<sup>1</sup>

<sup>1</sup>Shaanxi Key Laboratory of Complex System Control and Intelligent Information Processing, Xi'an University of Technology, Xi'an 710048, China

<sup>2</sup>School of Electronic and Electrical Engineering, Baoji University of Arts and Sciences, Baoji 721016, China

(Received 27 October 2022; revised manuscript received 14 November 2022; accepted manuscript online 22 November 2022)

The weak signal detection method based on stochastic resonance is usually used to extract and identify the weak characteristic signal submerged in strong noise by using the noise energy transfer mechanism. We propose a novel composite multistable stochastic-resonance (NCMSR) model combining the Gaussian potential model and an improved bistable model. Compared with the traditional multistable stochastic resonance method, all the parameters in the novel model have no symmetry, the output signal-to-noise ratio can be optimized and the output amplitude can be improved by adjusting the system parameters. The model retains the advantages of continuity and constraint of the Gaussian potential model and the advantages of the improved bistable model without output saturation, the NCMSR model has a higher utilization of noise. Taking the output signal-to-noise ratio as the index, weak periodic signal is detected based on the NCMSR model in Gaussian noise and  $\alpha$  noise environment respectively, and the detection effect is good. The application of NCMSR to the actual detection of bearing fault signals can realize the fault detection of bearing inner race and outer race. The outstanding advantages of this method in weak signal detection are verified, which provides a theoretical basis for industrial practical applications.

**Keywords:** weak signal detection, composite multistable, stochastic resonance, bearing fault detection

**PACS:** 02.60.Cb, 05.40.-a, 05.40.Fb, 05.45.-a

**DOI:** 10.1088/1674-1056/aca4bd

## 1. Introduction

With the rapid development of science and technology, weak characteristic signal detection has been widely used in many fields, such as communication,<sup>[1]</sup> seismic survey,<sup>[2]</sup> acoustics,<sup>[3]</sup> biomedical signal processing,<sup>[4]</sup> image processing,<sup>[5]</sup> and mechanical fault diagnosis.<sup>[6,7]</sup> As a comprehensive technology, weak signal detection integrates mathematics, electronics, nonlinear science, computer technology, and signal processing,<sup>[8–13]</sup> forming a new technology for extracting useful signals from strong noise. Due to the importance and universality of this problem, researchers continue to study the theory and method of weak signal detection to detect weak signal under strong noise background more quickly and accurately under certain constraints, or enhance the useful signal which is very weak in detection itself. At present, weak signal detection has developed into an important branch in the field of signal processing. The weak signal detection under strong noise mainly includes linear and nonlinear detection methods.<sup>[14,15]</sup> The linear method damages the useful signal while suppressing noise, resulting in loss of signal, so researchers have paid more attention to the nonlinear detection method. As a nonlinear method, stochastic resonance (SR) breaks the original idea that noise is always harmful. It uses the potential function of a nonlinear system to convert part of the noise energy into useful signal energy, thus using the noise to enhance detection of weak signals.<sup>[16,17]</sup> At the same time,

the SR method can realize weak signal detection by applying noise or adjusting system parameters. Therefore, SR has been developed rapidly and has achieved many achievements. The detection effect of the SR method has a great relationship with the nonlinear model. The early research on the SR model mainly revolves around the classic bistable stochastic resonance (CBSR) model. With the continuous deepening of theoretical and application research of the CBSR, it was found that the output of the CBSR model is easy to be saturated and the potential barrier of the potential function is high.<sup>[18]</sup> Zhao *et al.* proved that the CBSR system has the characteristic of output saturation.<sup>[19]</sup> Gosak *et al.* proposed a piecewise nonlinear bistable stochastic resonance (PNBSR) model for SR saturation which achieved certain results, but did not break the output saturation characteristic of CBSR.<sup>[20]</sup> Jiao *et al.* proposed an SR-based novel potential well (NPWSR) model, compared with the traditional model, this model has a lower potential barrier height, and the potential well wall is linearized. Under the same conditions, the NPWSR model solves the problems of high potential barrier and output saturation of the CBSR model, and the output signal-to-noise ratio (SNR) curve is higher than that of the CBSR method.<sup>[21]</sup> The Gaussian potential (GP) model is a special single potential well structure, which has the advantages of continuity and confinement. The depth and width of the potential well can be adjusted independently.<sup>[22]</sup> Combined with the bistable and

<sup>†</sup>Corresponding author. E-mail: gaorui@bjwxy.edu.cn

tristable models, it forms a tristable model with better performance stable and composite multistable systems. Zhang *et al.* proposed a tristable system model by combining GP model with bistable system, and verified that the detection result of this system for weak signals is better than that of a bistable system.<sup>[23]</sup> Jiao *et al.* proposed composite multistable SR on the basis of traditional tristable SR combined with GP, and proved that the performance of composite multistable SR is better than that of traditional tristable SR.<sup>[24]</sup> He *et al.* analyzed the characteristics of tri-stable stochastic resonance under Levy noise.<sup>[25]</sup> To further improve the weak signal detection performance of the system, we can make full use of the advantages of the GP model and the improved bistable SR model to build a better system model to make it easier for particles to transition. Therefore, the GP model and the piecewise linear models are combined to build a novel composite multistable SR (NCMSR) model, and based on this model, it is the most representative for Gaussian noise<sup>[26,27]</sup> and  $\alpha$  stable noise (also known as Levy noise),<sup>[28,29]</sup> the SR phenomenon was studied in a noisy environment, and the outstanding advantages of the new method in weak signal detection were verified.

The rest of this paper is organized as follows. In Section 2, a novel composite multistable SR model is proposed, and the detection performance of the novel model SR system is analyzed. In Section 3, the effect of system parameters on the output effect of SR driven by periodic signal is analyzed with the output SNR as the output measurement indicators, and the detection of weak periodic signal under Gaussian noise and  $\alpha$  noise environment is realized and applied to bearing fault detection. Conclusions are drawn in Section 4.

## 2. The system model

### 2.1. The GP model

The GP model is generally used to describe the scattering, and its expression<sup>[30]</sup> is

$$U_G(x) = -v \exp\left(-\frac{x^2}{r^2}\right), \quad (1)$$

where  $v$  is the depth,  $r$  is the width potential well. Figure 1 shows the shapes of the GP model under the action of different parameters when  $v = 1$  and when  $r = 1$ .

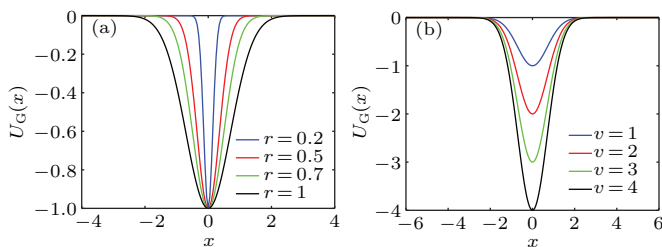


**Fig. 1.** The  $U_G(x)$  under different parameters: (a)  $U_G(x)$  for different  $r$  when  $v = 1$ , (b)  $U_G(x)$  for different  $v$  when  $r = 1$ .

### 2.2. The improved segment potential well model

The potential function expression of the improved segment model<sup>[31]</sup> is given as

$$U_1(x) = \begin{cases} \frac{-\sqrt{2}U_0}{m}(x+m) - U_0 - A_p x, & x < -m, \\ -\frac{a}{2}x^2 + \frac{b}{4}x^4 - A_p x, & -m \leq x < 0, \\ -\frac{a}{2}x^2 + \frac{b}{4}x^4 + A_p x, & 0 \leq x \leq m, \\ \frac{\sqrt{2}U_0}{m}(x-m) - U_0 + A_p x, & x > m, \end{cases} \quad (2)$$

where  $a$  and  $b$  are model parameters,  $m = \sqrt{a/b}$ ,  $U_0 = \sqrt{a^2/4b}$ ,  $A_p = l \cdot A_c$ ,  $0 \leq l \leq 1$ . Figure 2 shows the potential function diagram of the segmented model. It can be seen intuitively from Fig. 2 that compared with the classical bistable model, the potential barrier height of this model is lower, and the potential well wall is linearized.

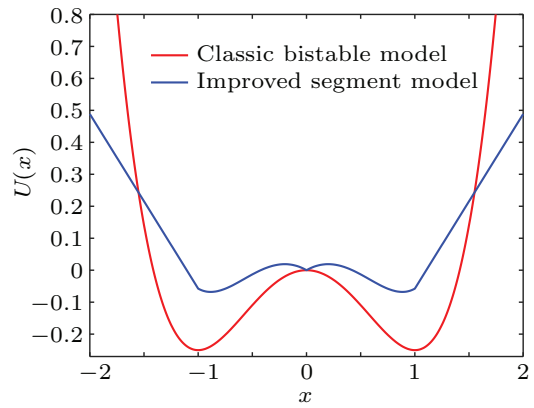


**Fig. 2.** The improved segment potential well model.

### 2.3. The NCMSR system

Combining the above-mentioned improved segmented model and the GP model, a novel type of the CMSR model is formed. The new model maintains the advantages of the two models, which reduces the potential barrier and is beneficial to the transition of particles. Its potential function is described in the following. When  $a = 2$ ,  $b = 1$ ,  $l = 0.5$ ,  $v = 0.06$ ,  $r = 0.1$ , the NCMSR potential well is shown in Fig. 3. At this time, we can adjust  $v$  and  $r$ , and locally adjust the potential function, so that the particles can achieve multi-step transitions, and we can fully convert the noise energy into useful signal energy.

When  $a = 2$ ,  $b = 1$ ,  $l = 0.5$ ,  $v = 0.06$ , and  $r = 1$ , the NCMSR potential function  $U(x)$  under the action of different  $v$  is shown in Fig. 4. The segment model is changed into a multistable model by adding the GP model, the reduction of potential barrier is conducive to the transition of particles. In Figs. 4(a) and 4(b), when  $v = 0.03$ , the depth of the intermediate potential well becomes smaller, and when  $v$  becomes larger, that is, when  $v = 0.06$  and  $0.08$ , it changes from tristability to multi-stability.

$$U(x) = U_1(x) - U_{G(x)} = \begin{cases} \frac{-\sqrt{2}U_0}{m}(x+m) - U_0 - A_p x + v \exp\left(-\frac{x^2}{r^2}\right), & x < -m, \\ \frac{-a}{2}x^2 + \frac{b}{4}x^4 - A_p x + v \exp\left(-\frac{x^2}{r^2}\right), & -m \leq x < 0, \\ \frac{-a}{2}x^2 + \frac{b}{4}x^4 + A_p x + v \exp\left(-\frac{x^2}{r^2}\right), & 0 \leq x \leq m, \\ \frac{\sqrt{2}U_0}{m}(x-m) - U_0 + A_p x + v \exp\left(-\frac{x^2}{r^2}\right), & x > m. \end{cases} \quad (3)$$

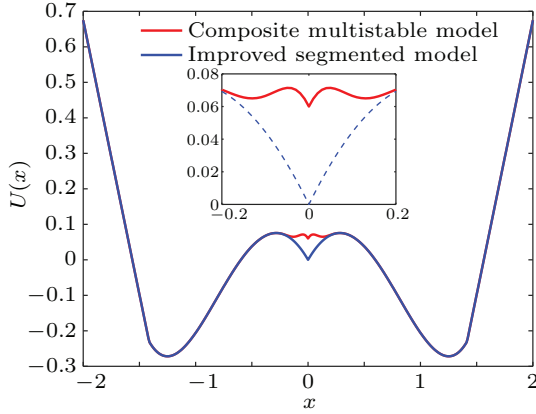


Fig. 3. The NCMSR potential well model.

The Langevin equation is a typical model describing an SR system under the joint action of weak periodic force and noise. It is derived from the collision mechanism of Brownian particle motion. The expression is given as follows:

$$\frac{dx}{dt} = -U'(x) + s(t) + \eta(t), \quad (4)$$

where  $x$  is the output of the SR system,  $U(x)$  is the potential function of the SR,  $s(t)$  is a periodic (aperiodic) signal,  $\eta(t) = \sqrt{2D}\xi(t)$ ,  $\xi(t)$  represents noise. Substituting Eq. (3)

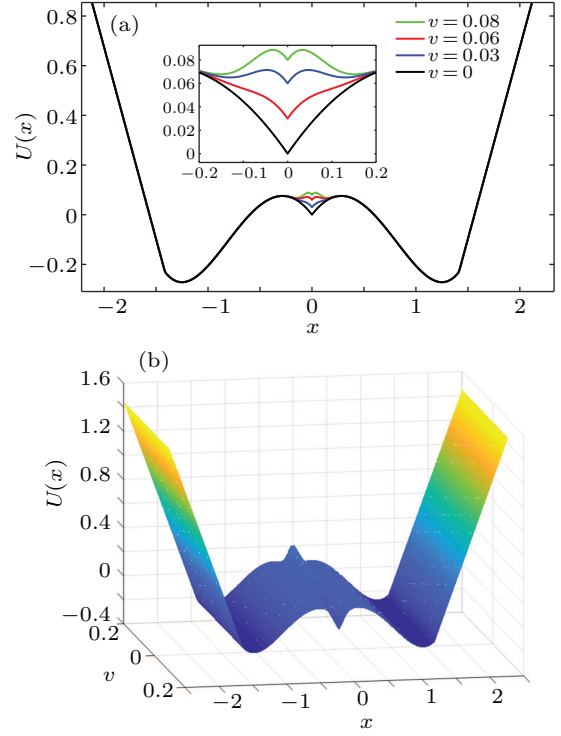
into Eq. (4) yields

$$\frac{dx}{dt} = \begin{cases} \frac{\sqrt{2}U_0}{m} + A_p + \frac{2vx}{r^2} \exp\left(-\frac{x^2}{r^2}\right) + s(t) + \eta(t), & x < -m, \\ ax - bx^3 + A_p + \frac{2vx}{r^2} \exp\left(-\frac{x^2}{r^2}\right) + s(t) + \eta(t), & -m \leq x < 0, \\ ax - bx^3 - A_p + \frac{2vx}{r^2} \exp\left(-\frac{x^2}{r^2}\right) + s(t) + \eta(t), & 0 \leq x \leq m, \\ -\frac{\sqrt{2}U_0}{m} - A_p + \frac{2vx}{r^2} \exp\left(-\frac{x^2}{r^2}\right) + \eta(t), & x > m. \end{cases} \quad (5)$$

Equation (5) is solved by fourth-order Runge Kutta algorithm to obtain the output of the SR system of the NCMSR model,<sup>[32]</sup> the obtained  $x$  is the output signal of the NCMSR system.

## 2.4. System parameter optimization algorithm

In this paper, the differential variation brain storming optimization (DBSO) algorithm is used to synchronously opti-


 Fig. 4.  $U(x)$  for fixed  $b = 5$ : (a)  $U(x)$  for different values of  $v$ , (b) three-dimensional profile of  $U(x)$  versus  $v$  and  $x$ .

mize multiple system parameters in a NCMSR system. Compared with other algorithms, the algorithm can give better consideration to both local and global search, and is not easy to fall into local optimization, thus effectively improving the performance of the algorithm. When the noisy signal is sent into the NCMSR system, the DBSO algorithm is used to synchronously optimize the structural parameters of the system. In order to match the optimal resonance model, the algorithm

takes the output SNR as the objective optimization function. When the SNR reaches the maximum value, a set of corresponding system parameters are obtained. Therefore, in the NCMSR system, the adaptive detection of weak signals is realized by adjusting parameters. The algorithm flow is shown in Fig. 5.

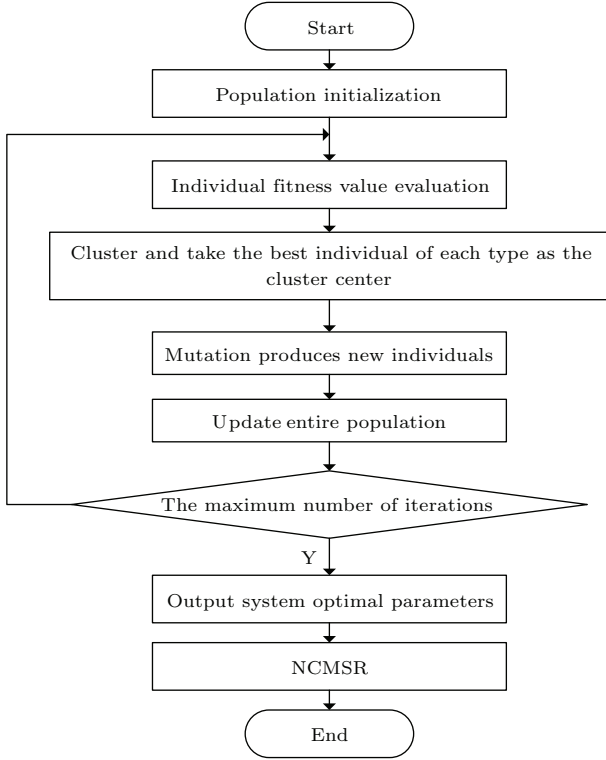


Fig. 5. Flow chart of adaptive NCMSR based on DBSO algorithm.

### 3. System simulation and engineering application

#### 3.1. Performance analysis of the NCMSR system

To further study the performance of the NCMSR system, the influence factors of NCMSR on periodic signals in Gaussian noise and  $\alpha$  stable noise environments are studied by taking the output SNR as a measurement index. Take periodic signal  $s(t) = A \sin(2\pi ft)$ ,  $A = 0.1$ ,  $f = 0.01$  Hz,  $N = 4096$ ,  $f_s = 4.08$  Hz,  $\mu = 0$ , and  $\sigma = 1$  for Gaussian noise,  $\alpha = 1.5$ ,  $\beta = 0$ ,  $\sigma = 1$ , and  $\mu = 0$  for  $\alpha$  stable noise. Figure 6 shows the curves of output SNR of the SR system versus  $D$ . The results shown are the average values of 10 experiments, the parameters of the two systems are  $(a, b, l, v, r) = (0.5, 0.3, 0.5, 0.06, 0.1)$  and  $(a, b, c) = (0.5, 0.3, 0.5)$ , respectively. Gaussian noise intensity range is  $[0, 4]$  and  $\alpha$  noise intensity range is  $[0, 1]$ . In Fig. 6, the output SNR of the NCMSR system is generally higher than that of the traditional tristable SR system in the two noise environments as a whole. This is because the NCMSR system can locally change the shape of the potential function by adjusting the parameters to achieve good synergy between

the system, noise and input signal, and fully realize the transformation from noise energy to signal energy, so as to highlight the characteristics of the signal to be measured.

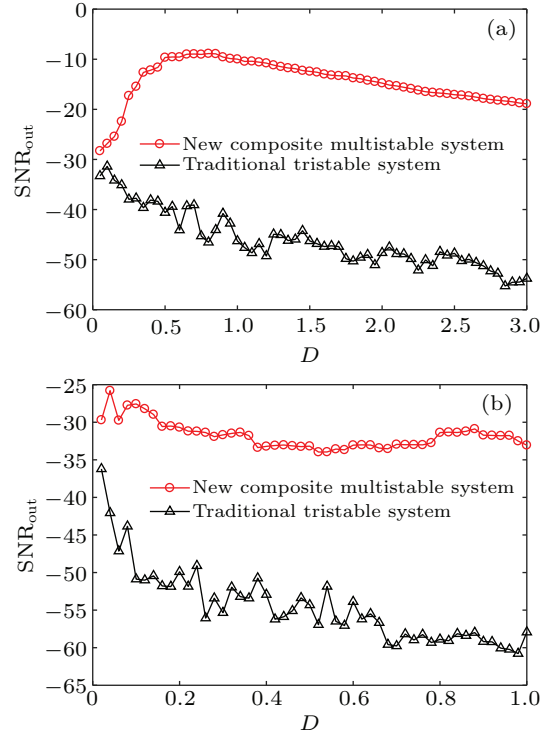


Fig. 6. Curves of SNR versus  $D$ : (a) variation curve in Gaussian noise environment, (b) variation curve in  $\alpha$  stable noisy environment.

#### 3.2. Performance analysis of the NCMSR model under Gaussian noise

In order to study the applicability of the NCMSR system to the detection of different periodic signals, periodic signals are used in the simulation, and the Gaussian noise and  $\alpha$  noise are used as the noise in simulation detection environment to analyze the parameter-induced SR driven by different periodic signals. Fixed Gaussian noise intensity  $D = 1.2$ , the number of sampling points  $N = 4096$ , the low frequency signal sampling frequency  $f_s = 4.08$  Hz, the high-frequency signal sampling frequency  $f_s = 40.8$  kHz, the NCMSR system parameter optimization range is set to  $a \in (0, 10]$ ,  $b \in (0, 10]$ ,  $l \in (0, 1]$ ,  $v \in (-0.5, 3]$ , and  $r \in (0, 3]$ .

##### 3.2.1. Single low frequency

Take the periodic signal to be measured as  $s(t) = A \sin(2\pi ft)$ ,  $A = 0.1$ ,  $f = 0.01$  Hz. The signal and noise are mixed to obtain a noisy signal with an input SNR of  $-25.1025$  dB. The time-domain diagram and power spectrum diagram of noisy signals are shown in Figs. 7(a) and 7(b), the noisy signal passes through the NCMSR system, using the DBSO optimization algorithm, the system optimization parameters can be obtained as  $a = 0.0675$ ,  $b = 0.0276$ ,  $l = 0.5433$ ,  $v = -0.4999$ , and  $r = 0.536$ , the system output



SNR of system is  $-5.3018$  dB, which is  $19.8007$  dB higher than the input SNR. The NCMSR system output time-domain diagram and power spectrum diagram are shown in Figs. 7(c) and 7(d).

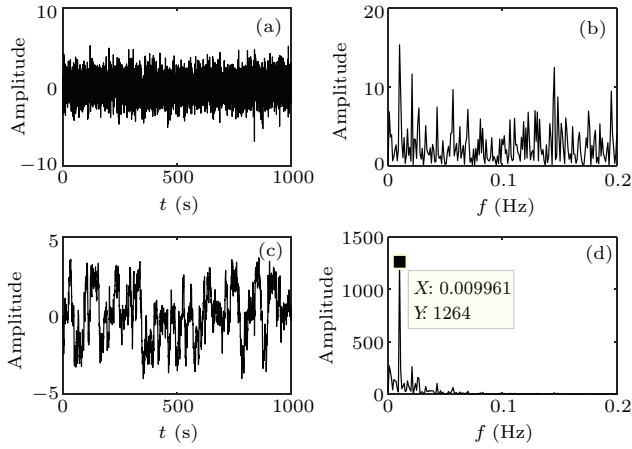


**Fig. 7.** Detection of single low frequency signal: (a) time domain diagram, (b) power spectrogram, (c) time-domain diagram, (d) power spectrogram.

### 3.2.2. Multiple low frequencies

The adaptive NCMSR driven by multiple low-frequency periodic signals is studied, the signal to be measured is  $s(t) = A_1 \sin(2\pi f_1 t) + A_2 \sin(2\pi f_2 t) + A_3 \sin(2\pi f_3 t)$ ,  $A = 0.1$ ,  $f_1 = 0.01$ ,  $f_2 = 0.02$ ,  $f_3 = 0.04$ , the signal and noise are mixed to obtain a noisy signal with an input SNR of  $-26.8176$  dB. Its time-domain diagram and power spectrum diagram are shown in Figs. 8(a) and 8(b). The noisy signal passes through the NCMSR system, using the DBSO optimization algorithm, the system optimization parameters can be obtained as  $a = 0.3998$ ,  $b = 0.2367$ ,  $l = 0.2983$ ,  $v = -0.3365$ , and  $r = 0.2879$ , when the output SNR is  $-8.862$  dB, which is  $17.9556$  dB higher than the input SNR. The NCMSR system output time-domain diagram and power spectrum diagram are shown in Figs. 8(c) and 8(d).

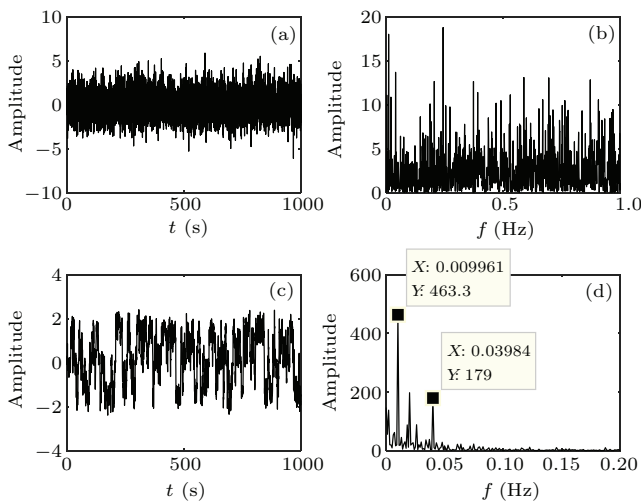


**Fig. 8.** Detection of multiple low frequency signals: (a) time-domain diagram, (b) power spectrogram, (c) time-domain diagram, (d) power spectrogram.

### 3.2.3. Single high frequency

In the actual mechanical fault signal detection, it is often a high-frequency signal, so it is of great significance for detection of high-frequency weak signals. In this paper, parameter compensated SR and adaptive NCMSR are combined to detect high-frequency signals. The signal to be measured is  $s(t) = A \sin(2\pi f t)$ ,  $A = 0.1$ ,  $f = 100$  Hz, and we mix the high frequency with noise to obtain a noisy signal with an input SNR of  $-24.0777$  dB. The time-domain diagram and power spectrum diagram are shown in Figs. 9(a) and 9(b), the noise signal is fed into the NCMSR system, using the DBSO optimization algorithm, the system optimization parameters can be obtained as  $a = 0.0969$ ,  $b = 0.0248$ ,  $l = 0.8369$ ,  $v = -0.192$ , and  $r = 0.4366$ . At this time, the output SNR is  $-1.6369$  dB, which is  $22.4408$  dB higher than the input SNR. The NCMSR system output time-domain diagram and power spectrum diagram are shown in Figs. 9(c) and 9(d).

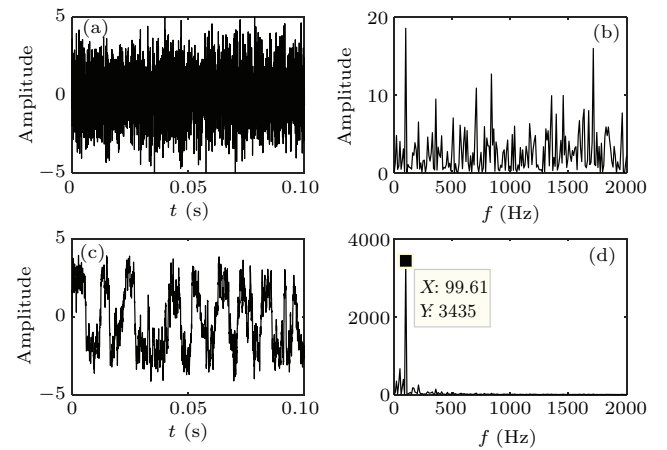


**Fig. 9.** Detection of single high frequency signal: (a) time domain diagram, (b) power spectrogram, (c) time-domain diagram, (d) power spectrogram.

### 3.2.4. Multiple high frequencies

When studying the SR driven by multiple high-frequency periodic signals, the signal to be measured is  $s(t) = A_1 \sin(2\pi f_1 t) + A_2 \sin(2\pi f_2 t) + A_3 \sin(2\pi f_3 t)$ ,  $A = 0.1$ ,  $f_1 = 100$ ,  $f_2 = 200$ , and  $f_3 = 400$ , the signal and noise are mixed to obtain a noisy signal with an input SNR of  $-25.1161$  dB. Figures 10(a) and 10(b) are the time-domain diagram and power spectrum diagram, the noisy signal is sent to the NCMSR system, using the optimization algorithm of DBSO, when the system optimization parameters are obtained as  $a = 0.0181$ ,  $b = 0.0182$ ,  $l = 0.9531$ ,  $v = -0.3539$ , and  $r = 1.0606$ . At this time, the system output SNR is  $-9.8461$  dB, which is  $15.27$  dB higher than the input SNR. The NCMSR system output time-domain diagram and power spectrum diagram are shown in Figs. 10(c) and 10(d).

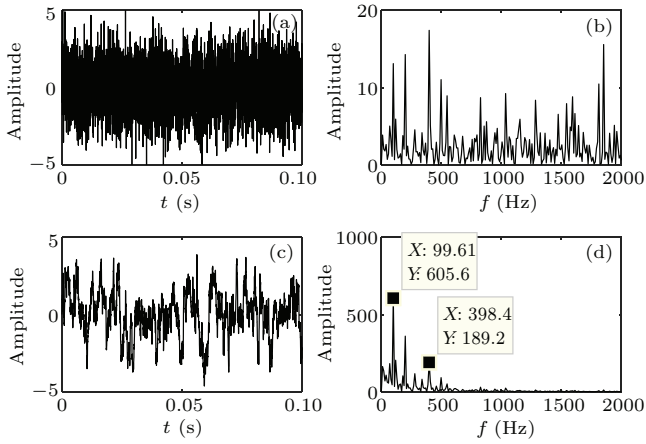


**Fig. 10.** Detection of multiple high frequency signals: (a) time domain diagram, (b) power spectrogram, (c) time-domain diagram, (d) power spectrogram.

From the time-domain diagrams (a) of Figs. 7–10, it can be seen that the periodic signal has been overwhelmed by noise, and the periodic waveform cannot be identified, the frequency corresponding to the periodic signal cannot be observed in the power spectrum (b). The output time-domain diagram (c) shows that after the noisy signal passes through the NCMSR system, the waveform of the output signal will be distorted to a certain extent, and it will no longer strictly follow the trajectory of the input signal, but in the output power spectrum diagram (d), the frequency close to the input signal frequency can be clearly observed, and the frequency has a higher spectral peak than the surrounding spurious spectrum, indicating that the SR system, signal and noise have achieved good matching, the periodic signal detection of single low frequency, multiple low frequencies, single high frequency and multiple high frequency is completed under Gaussian noise.

### 3.3. Performance analysis of the NCMSR model under $\alpha$ noise

The periodic signal in the Gaussian noise environment is tested above, and it is verified that the NCMSR has better performance, but the  $\alpha$  stable noise generated by the simulation has the characteristics of spikes in the actual noise, so the  $\alpha$  stable noise is compared with Gaussian white noise, it can describe the actual noise environment well and is closer to the practical application. Here,  $\alpha$  noise fixed intensity  $D = 0.3$ , the number of sampling points  $N = 4096$ , the low-frequency-signal sampling frequency  $f_s = 4.08$  Hz, the high-frequency-signal sampling frequency  $f_s = 40.8$  kHz, the NCMSR system parameter optimization range is set to  $a \in (0, 10]$ ,  $b \in (0, 10]$ ,  $l \in (0, 1]$ ,  $v \in (-0.5, 3]$ , and  $r \in (0, 3]$ .

#### 3.3.1. Single low frequency

In  $\alpha$  stable noise environment, the influence of the NCMSR system on the periodic signal is analyzed by using the SNR as a measure. Take the periodic signal to be measured as  $s(t) = A \sin(2\pi ft)$ ,  $A = 0.3$ ,  $f = 0.01$  Hz, and mix the signal

with the noise to obtain a noisy signal with an input SNR of  $-26.02$  dB. The time-domain diagram and power spectrum diagram are shown in Figs. 11(a) and 11(b), the noisy signal is sent to the NCMSR system, using the DBSO optimization algorithm, the system optimization parameters can be obtained as  $a = 0.4105$ ,  $b = 0.0878$ ,  $l = 0.0018$ ,  $v = -0.5$ , and  $r = 1.0029$ , the output SNR is  $-1.0527$  dB, an improvement of  $24.9673$  dB compared with the input SNR. The NCMSR system output time-domain diagram and power spectrum diagram are shown in Figs. 11(c) and 11(d).

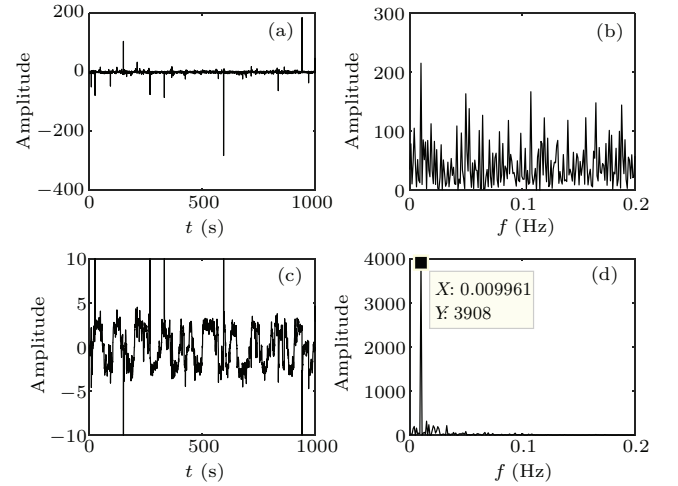


**Fig. 11.** Detection of single low frequency signal: (a) time domain diagram, (b) power spectrogram, (c) time-domain diagram, (d) power spectrogram.

#### 3.3.2. Multiple low frequencies

When studying the SR driven by multiple low-frequency periodic signals, the signal to be tested is selected as  $s(t) = A_1 \sin(2\pi f_1 t) + A_2 \sin(2\pi f_2 t) + A_3 \sin(2\pi f_3 t)$ ,  $A = 0.3$ ,  $f_1 = 0.01$ ,  $f_2 = 0.02$ ,  $f_3 = 0.04$ , the signal and noise are mixed to obtain noisy signals with an input SNR of  $-26.8215$  dB, the time-domain diagram and power spectrum diagram are shown in Figs. 12(a) and 12(b).

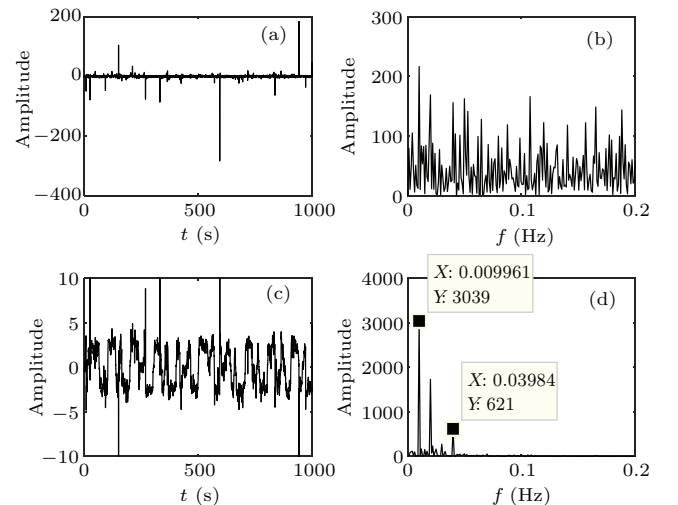


**Fig. 12.** Detection of multiple low frequency signals: (a) time domain diagram, (b) power spectrogram, (c) time-domain diagram, (d) power spectrogram.

The noisy signal is sent into the NCMSR system, using the DBSO optimization algorithm, the system optimization parameters can be obtained as  $a = 0.3261$ ,  $b = 0.0742$ ,  $l = 0.0001$ ,  $v = -0.5$ ,  $r = 0.7842$ , and the output SNR is  $-4.6466$  dB, which is  $22.1849$  dB higher than the input SNR. The NCMSR system output time-domain diagram and power spectrum diagram are shown in Figs. 12(c) and 12(d).

### 3.3.3. Single high frequency

The actual mechanical fault signals are all high-frequency signals, a single high-frequency signal is taken as the research object under noise. Take the periodic signal to be measured as  $s(t) = A \sin(2\pi ft)$ ,  $A = 0.3$ ,  $f = 100$  Hz, and mix the signal with noise to obtain a noise-containing signal with an input SNR of  $-26.02$  dB. The time-domain diagram and power spectrum diagram are shown in Figs. 13(a) and 13(b). Send the noisy signal into the NCMSR system, using the DBSO optimization algorithm, the system optimization parameters can be obtained as  $a = 0.0439$ ,  $b = 0.0184$ ,  $l = 0.853$ ,  $v = -0.2089$ , and  $r = 0.0037$ . The output SNR is  $-1.2018$  dB, the SNR is increased by  $24.8182$  dB compared with the input signal. The NCMSR system output time-domain diagram and power spectrum diagram are shown in Figs. 13(c) and 13(d).

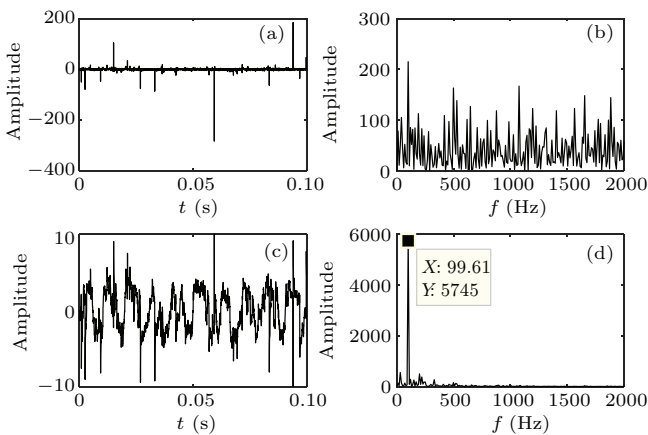


**Fig. 13.** Detection of single high frequency signal: (a) time domain diagram, (b) power spectrum, (c) time-domain diagram, (d) power spectrum.

### 3.3.4. Multiple high frequencies

When studying the SR driven by multiple high-frequency periodic signals, the signal to be tested is selected as  $s(t) = A_1 \sin(2\pi f_1 t) + A_2 \sin(2\pi f_2 t) + A_3 \sin(2\pi f_3 t)$ ,  $A = 0.3$ ,  $f_1 = 100$ ,  $f_2 = 200$ , and  $f_3 = 400$ , the signal and noise are mixed to obtain a noisy signal with an input SNR of  $-26.8215$  dB. The time-domain diagram and power spectrum diagram are shown in Figs. 14(a) and 14(b), and the noisy signal is sent into the NCMSR system, using the DBSO optimization algorithm, the system optimization parameters can be obtained

as  $a = 0.3501$ ,  $b = 0.0744$ ,  $l = 0.0001$ ,  $v = -0.5537$ , and  $r = 0.8841$ , when the output SNR is  $-4.6368$  dB, which is  $22.1947$  dB higher than the input SNR. The NCMSR system output time-domain diagram and power spectrum diagram are shown in Figs. 14(c) and 14(d).

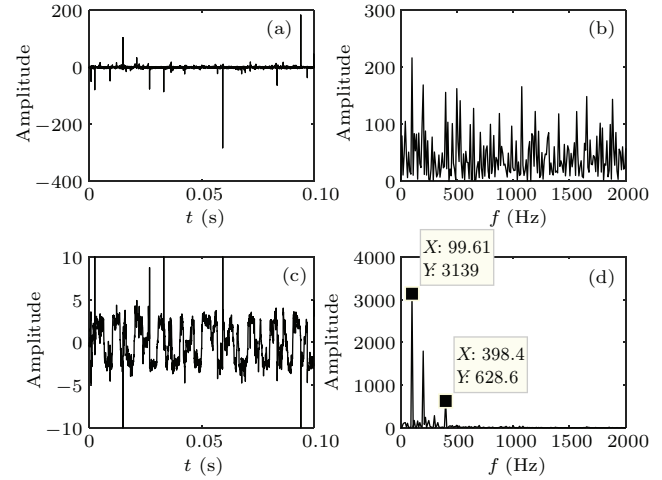


**Fig. 14.** Detection of multiple high frequency signals: (a) time domain diagram, (b) power spectrum, (c) time-domain diagram, (d) power spectrum.

It can be seen that the periodic signal has been submerged by noise, and the periodic waveform cannot be identified from the time-domain diagrams (a) of Figs. 11–14, the frequency of the periodic signal cannot be observed in the power spectrum diagram (b). The output time-domain diagram (c) shows that after the NCBSR system, the waveform of the output signal will have a certain distortion and no longer strictly follow the trajectory of the input signal, but in the output power spectrum diagram (d), the frequency close to the input signal frequency can be clearly observed, and the frequency has a higher spectral peak than the surrounding spurious spectrum, indicating that the signal, noise and SR system have achieved good matching, and the single low frequency under  $\alpha$  noise has been completed, multiple low frequency, single high frequency, multiple high frequency periodic signal detection.

### 3.4. Comparison with traditional tristable SR model

To more clearly show the advantages of the NCMSR model in weak signal detection, take the single low periodic signal with extremely small amplitude as an example for detection, given Gaussian noise, take the weak signal amplitudes as  $0.1$ ,  $0.01$ ,  $0.001$ , and  $0.0001$ , the comparison results of the two system are shown in Table 1. It can be seen that the SNR output of the NCBSR system is greater than that of the traditional tristable system. It shows that the NCMSR system is superior to the traditional tristable system in detecting low frequency weak signals with very small amplitude.



**Table 1.** Output SNR comparisons of different systems.

	Signal amplitude $v$	Input SNR (dB)	System type	System parameters					Output SNR (dB)	Increase (dB)
				$a$	$b$	$l$	$v$	$r$		
1	0.1	−30.64	NCMSR	0.46	0.14	0.02	−0.32	0.30	−2.67	27.97
			Traditional tristable	0.68	1.06	0.57			−4.36	26.28
2	0.01	−30.89	NCMSR	5.85	3.07	0.21	0.92	1.49	−5.22	25.67
			Traditional tristable	1.65	1.92	13.01			−5.31	25.58
3	0.001	−29.89	NCMSR	0.38	1.90	0.82	1.03	1.79	−6.04	23.85
			Traditional tristable	0.69	4.34	69.68			−6.45	23.44
4	0.0001	−29.80	NCMSR	5.68	4.11	0.01	1.69	0.44	−5.60	24.2
			Traditional tristable	0.77	4.21	64.10			−6.62	23.18

### 3.5. Engineering application

The actual bearing fault data is from XJTU-SY Bearing Datasets of Xi'an Jiaotong University. The data set includes the complete operation failure data of 15 rolling bearings from

the bearing test bench.<sup>[33]</sup> Select the fault signal of bearing drive end as the signal to be tested. The test bearing model selected in this paper is LDK UER204 rolling bearing.<sup>[34]</sup> Table 2 shows the main parameters of the bearing.

**Table 2.** LDK UER204 bearing parameters.

Inner ring diameter $d_1$ (mm)	Outer ring diameter $d_2$ (mm)	Middle diameter of bearing $D$ (mm)	Ball diameter $d$ (mm)	Number of balls, $n$	Contact angle $\alpha$ (°)
29.30	39.80	34.55	7.92	8	0

The sampling frequency is set as  $f_s = 25.6$  kHz, the bearing speed is  $r = 2400$  r/min (frequency conversion  $f_r = 39.29$ ). In the case of bearing failure, the theoretical values of the fault characteristic frequency of the inner and outer rings are calculated by Eqs. (1) and (2).<sup>[35]</sup>

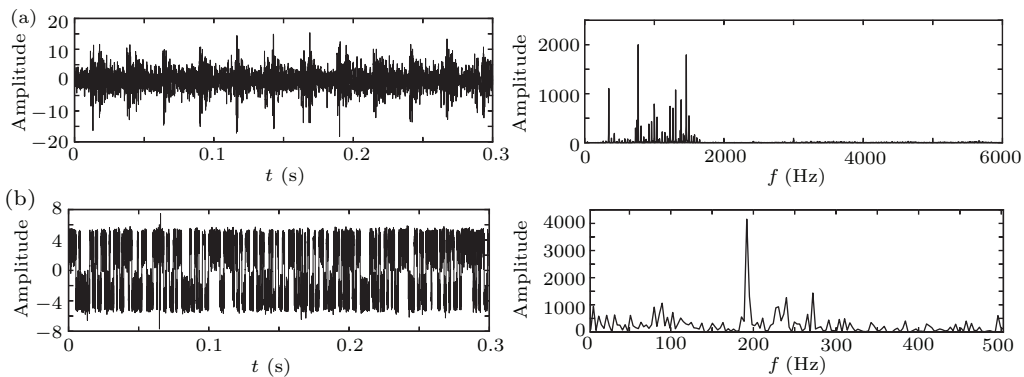
$$f_1 = r/60 \times 1/2 \times n(1 + d/D \times \cos \alpha) = 196.68 \text{ Hz}, \quad (6)$$

$$f_0 = r/60 \times 1/2 \times n(1 - d/D \times \cos \alpha) = 123.32 \text{ Hz}. \quad (7)$$

### 3.6. Fault diagnosis of bearing inner race

The time-domain diagram and power spectrum diagram of the sampled bearing inner race fault data are shown in Fig. 15(a),  $N = 8000$ , the input SNR of bearing inner race fault

signal is −35.4473 dB. Input the fault signal after high pass filtering into the NCMSR system, and obtain a group of system parameters through DBSO algorithm as follows:  $a = 4.9334$ ,  $b = 0.1435$ ,  $c = 0.0043$ ,  $v = 2.2763$ , and  $r = 3.0000$ . The output SNR is −16.3941 dB, the system output signal is shown in Fig. 15(b), the time-domain diagram shows that the output signal waveform has certain periodicity. In its power spectrum, a peak with amplitude significantly greater than that of the surrounding clutter spectrum is observed at  $f = 195.48$  Hz. There is a small error of 1.2 Hz with the theoretical value  $f = 196.68$  Hz, and the fault characteristic frequency can be identified.


**Fig. 15.** Inner ring fault signal detection: (a) inner ring fault signal, (b) output signal of NCMSR.

#### 3.6.1. Fault diagnosis of bearing outer race

The time-domain diagram and power spectrum diagram of the sampled bearing inner race fault data are shown in

Fig. 16(a),  $N = 8000$ , the input SNR of bearing inner race fault signal is −15.1889 dB. The filtered fault signal is input into the NCMSR system, and a group of system parameters are obtained through DBSO algorithm optimization:  $a = 3.3792$ ,

$b = 0.0765$ ,  $c = 0.0001$ ,  $v = 1.7951$ , and  $r = 2.2730$ . The output SNR is  $-8.6922$  dB, the output signal through the NCMSR system is shown in Fig. 16(b). The time-domain diagram system output signal has certain periodicity, in its power spectrum, a peak with amplitude significantly greater than the

surrounding clutter spectrum is observed at  $f = 124.8$  Hz, and the fault characteristic frequency can be identified, but there is a small error of  $1.48$  Hz with the theoretical value of  $f_1 = 123.32$  Hz. Therefore, the NCMSR system realizes the detection of the fault signal of the bearing outer ring.

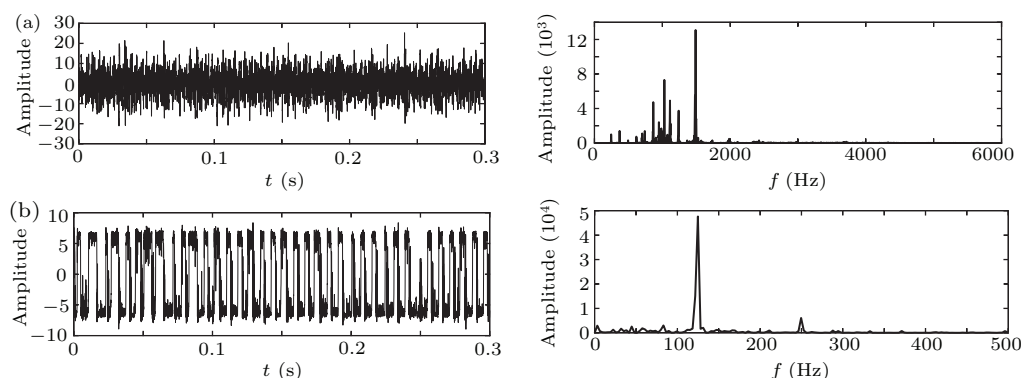


Fig. 16. Outer ring fault signal detection: (a) outer ring fault signal, (b) output signal of NCMSR.

## 4. Conclusion and perspectives

This paper focuses on an NCMSR model which solves the shortcomings of traditional bistable SR, such as high barrier and easy saturation, and the shortcomings of the traditional tristable method that the intermediate parameters are not easy to adjust. This model combines GP with the improved piecewise bistable. The NCMSR system can adaptively adjust the structural parameters of the nonlinear system according to the different signals to be measured with noise, so as to detect weak useful signals submerged in strong noise. There are four research results: (1) The NCMSR model is constructed on the basis of the GP model and the improved segment model, the NCMSR system driven by periodic signal can generate SR by the parameter-induced method, and the influence of NCMSR noise intensity on system output SNR is analyzed. (2) In the environment of Gaussian noise and  $\alpha$  noise, the NCMSR system detects single low frequency, multiple low frequencies, single low frequency, and multiple high frequency periodic signals, and has good output detection effect. (3) The experimental results show that the NCMSR model has better system performance than the traditional tristable SR model. (4) The application of NCMSR to the actual detection of bearing fault signals can realize the fault detection of bearing inner race and outer race. Based on the above analysis, the NCMSR system can enhance the detection effect of weak signals, and has better weak signal processing ability. In the next step, this model can be applied to the detection of non periodic signals, image enhancement, and medical ECG signal detection. The models and methods studied in this paper further enrich the SR theory and provide more possibilities for the detection of weak characteristic signals in practical engineering fields.

## Acknowledgements

Project supported by the National Natural Science Foundation of China (Grant No. 61871318), the Key Research and Development Projects in Shaanxi Province (Grant No. 2023-YBGY-044), and the Key Laboratory System Control and Intelligent Information Processing (Grant No. 2020CP10).

## References

- [1] Guo Y T, Zhou P, Yao Z and Ma J 2021 *Nonlinear Dyn.* **105** 3603
- [2] Zhou Z B, Yu W X, Wang J N and Liu M T 2022 *Chaos, Solitons & Fractals* **154** 111642
- [3] Mba C U, Makis V, Marchesiello S, Fasana A and Garibaldi L 2018 *Measurement* **126** 76
- [4] Li J M, Wang X D and Zhang X D 2021 *Nonlinear Dyn.* **104** 971
- [5] Qiao Z J, Elhatab A, Shu X D and He C B 2021 *Nonlinear Dyn.* **106** 707
- [6] Yang Y B, Tao W M, Huang J M and Xu B H 2012 *Chin. Phys. B* **21** 060503
- [7] Qiao Z J and Shu X D 2021 *Chaos, Solitons and Fractals* **145** 110813
- [8] Mcnamara B, Wiesenfeld K and Roy R 1988 *Phys. Rev. Lett.* **60** 2626
- [9] He M, Xu W and Sun Z 2015 *Nonlinear Dyn.* **79** 1787
- [10] Zhong S, Zhang L, Wang H, Ma H and Luo M 2017 *Nonlinear Dyn.* **89** 1327
- [11] Kim H, Tai W C, Zhou S X and Zuo L 2017 *Smart Mater. Struct.* **26** 115011
- [12] Lu S, He Q and Wang J 2019 *Mech. Syst. Signal Process.* **116** 230
- [13] Zhang G, Song Y and Zhang T Q 2017 *Chin. J. Phys.* **55** 85
- [14] Jin Y F 2018 *Chin. Phys. B* **27** 050501
- [15] Liu H G, Liu X L, Yang J H, Sanjuan M A F and Cheng G 2017 *Nonlinear Dyn.* **89** 2621
- [16] Yao Y G 2021 *Chin. Phys. B* **30** 060503
- [17] Shi T T, XU X M, Sun K H, Ding Y P and Huang W G 2020 *Chin. Phys. B* **29** 050501
- [18] Qiao Z J, Lei Y G, Lin J and Jia F 2017 *Mech. Syst. Signal Process.* **84** 731
- [19] Wang Z J and Wang L 2013 *Chaos* **23** 33117
- [20] Goask M, Perc M and Kralj S 2011 *Eur. Phys. J. B* **80** 519
- [21] Jiao S B, Lei S, Jiang W, Zhang Q and Huang W C 2019 *IEEE Access* **7** 160191
- [22] Du T H, Cheng X, Sun S G, Hao J, Wang R X and Liang J 2020 *Instrument Technique and Sensor* **450(07)** 100 (in Chinese)
- [23] Zhang G and Gao J P 2018 *Comput. Appl.* **38** 2747 (in Chinese)

- [24] Jiao S B, Qiao X X, Lei S and Jiang W 2019 *Chin. J. Phys.* **59** 138
- [25] He L F, Cui Y Y, Zhang T Q, Zhang G and Song Y 2016 *Chin. Phys. B* **25** 060501
- [26] He Q B, Wu E H and Pan Y Y 2018 *J. Sound Vibr.* **420** 174
- [27] Li J M, Chen X F, Du Z H, Fang Z W and He Z J 2013 *Renew. Energy* **60** 7
- [28] Zeng L Z and Xu B H 2010 *J. Phys. A: Statist. Mech. Appl.* **389** 5128
- [29] Han D Y, Su X and Shi P M 2018 *Chin. J. Phys.* **56** 1559
- [30] Zhang H B, He Q, Lu S and Kong F 2014 *Math. Problems Eng.* **2014** 315901
- [31] Ma T C, Xu F Y, Hu J Z, Song D and Cao S S 2021 *Chin. J. Phys.* **74** 279
- [32] Wang Y, Jiao S B, Zhang Q, Lei S and Qiao X X 2018 *Chin. J. Phys.* **56** 1187
- [33] Wang B, Lei Y G, Li N P and Li N B 2020 *IEEE Trans. Reliab.* **69** 401
- [34] Lei Y G, Han T Y and Wang B 2019 *J. Mech. Eng.* **55** 1 (in Chinese)
- [35] Zhang G, Hu D and Zhang T 2019 *IEEE Access* **7** 58435